The 8th International Supercritical CO_2 Power Cycles Symposium
February 27 – 29, 2024, San Antonio, Texas
Paper #20

A method to develop centrifugal compressor performance maps for off-design and dynamic simulation studies of sCO_2 cycles

Colin du Sart, Pr Eng
Mechanical Engineering
University of Cape Town
Cape Town, South Africa

Pieter Rousseau, Pr Eng
Mech. & Mechatronic Eng.
Stellenbosch University
Stellenbosch, South Africa

Ryno Laubscher, Pr Eng
Mech. & Mechatronic Eng.
Stellenbosch University
Stellenbosch, South Africa

Colin du Sart is a professionally registered engineer and financial analyst. Colin is currently completing a PhD in solar thermal sCO_2 power plants while lecturing courses in thermofluid sciences. Before moving into academia, Colin worked as a project engineer for Paterson & Cooke Consulting Engineers.

Pieter Rousseau is a full-time professor and ex CEO of M-Tech Industrial (Pty) Ltd who specializes in the simulation and optimisation of thermofluid systems. Pieter has over 150 publications, has held numerous senior research positions during his career, has pioneered several innovative commercial thermofluid systems and was part of the team that originally developed the Flownex® SE software.

Ryno Laubscher is a full-time associate professor who specializes in the use of computational fluid dynamics and machine learning to model thermofluid systems. Ryno has over 40 publications and many years of industrial experience, having previously worked for John Thompson and Enexio GmbH.

Abstract

There is a growing interest in the use of supercritical carbon dioxide (sCO_2) Brayton cycles for power generation applications. Consequently, many researchers have developed cycle-only models, or plant models at various levels of detail to study the feasibility of such technologies. In these studies, the compressor model used has a significant effect on the results obtained. Despite this, many researchers specify a constant isentropic efficiency, or adopt the efficiency and head correlation curves presented by Dyreby, which is based on the performance maps of a compressor developed for Sandia National Laboratories (SNL). The former approach is only suitable for steady state design point studies, and Dyreby's correlations are not meant to be

scaled. Furthermore, Dyreby's correlations may be employed without considering the velocities of the fluid, which is critical for the determination of fluid properties throughout the turbomachine. Therefore, neither approach is suitable for off-design or dynamic studies but are used regardless because of the limited public data available on sCO_2 turbomachinery. In this paper, a method is presented which may be used to size a single stage centrifugal (or radial) compressor for given nominal boundary conditions, and to develop performance maps for the same compressor at off-design conditions. These maps may then be employed to perform off-design and dynamic studies. The method employs a one-dimensional mean-line analysis approach with enthalpy loss correlations and has been verified using data from the SNL compressor. Additionally, case studies are presented where the method is used to produce conceptual designs for compressors for a proposed 50 MWe sCO_2-CSP plant.

Nomenclature

Normal symbols		η^*	Modified efficiency
A	Flow area in m^2	ν	Kinematic viscosity in m^2/s
c	Fluid velocity in m/s	ω	Angular velocity in rad/s
D	Diameter in meter	ϕ	Flow coefficient
d_s	Specific diameter	ϕ^*	Modified flow coefficient
h	Specific enthalpy in J/kg	ψ	Head coefficient
$\dot{m}$	Mass flow rate in kg/s	ψ^*	Modified head coefficient
N	Rotational speed in rpm	ρ	Density in kg/m^3
n_s	Specific speed	**Subscripts**	
P	Pressure in Pa	0	Guide vanes inlet, or stagnation
r	Radius in meter	1	Impeller inlet
ss	Speed of sound in m/s	2	Impeller exit
T	Temperature in Kelvin or °C	3	Vaned diffuser inlet
u	Blade velocity in m/s	4	Vaned diffuser exit
$\dot{V}$	Volume flow rate in m^3/s	5	Volute/ collector exit
w_c	Compressor specific work in J/kg	nom	Nominal/ design condition
w_{Euler}	Euler specific work in J/kg	s or ss	Isentropic
Greek symbols		TT	Total-to-total
Δ	Difference	TS	Total-to-static
η	Efficiency	t	Tangential direction

1. Introduction and literature review

Supercritical carbon dioxide (sCO_2) power cycles exhibit a simpler cycle layout with smaller turbomachinery and increased thermal efficiency when compared to Rankine cycles, and air or helium Brayton cycles (Brun, Friedman & Dennis, 2017). However, there are no utility-scale or commercially operating sCO_2 plants. If sCO_2 power cycles are to be applied in power plants in future, there is a need to determine what these plants should look like and how they should be

operated. Part of this includes the design of the compressor(s), how they are modelled, and how they affect the dynamic behavior of the plant. The following sections reviews the traditional approaches used to model sCO_2 compressors.

1.1. Constant isentropic efficiency model

Numerous studies have employed a constant isentropic efficiency compressor model to investigate the performance of sCO_2 cycles. These include cycle design point studies by Kulhanek & Dostal (2011), Turchi et al. (2013) and Neises & Turchi (2014) to name a few, who used a commonly assumed isentropic efficiency of 89%. For concentrated solar power (CSP) applications, Padilla, Benito & Stein (2015) employed a constant isentropic efficiency in a steady state exergy analysis of an sCO_2 cycle coupled with a direct-heat CSP tower system. Furthermore, also for CSP applications, numerous studies employed a constant isentropic efficiency for off-design studies. Seidel (2010) performed quasi-steady state monthly and annual simulations of a simple sCO_2 cycle to assess its suitability for use as the power block in CSP systems. Osorio, Hovsapian & Ordonez (2016) studied the behavior of a CSP plant incorporating an sCO_2 Brayton cycle with multiple stages of reheating and intercooling, and with and without recuperation. Binotti et al. (2017) investigated the performance of a CSP plant incorporating thermal energy storage (TES) and a recompression cycle with intercooling over the course of a year. Following a series of parametric studies, Luu et al. (2017a) proposed two cycle control strategies for changing solar energy availability. Finally, Neises & Turchi (2019) compared the performance and cost of sCO_2-CSP tower plants incorporating TES. The use of a constant isentropic efficiency model is therefore widely accepted for steady state studies. The model has also been used for quasi-steady state studies. However, this model is only suitable for design point steady state studies, since the isentropic efficiency of a compressor varies for different operating conditions (inlet fluid properties, flow rates and operating speeds).

1.2. SNL compressor based model

Few researchers have completed off design studies using a more detailed compressor model. From the literature reviewed, the majority of these studies use non-dimensional efficiency and head coefficient performance curves (or correlations) proposed by Dyreby (2014), given in Equations (1) to (5). These correlations are semi-empirical curve fits, derived from performance maps and experimental data for the unshrouded centrifugal (or radial) main compressor used in the sCO_2 experimental rig at Sandia National Laboratories (SNL). Consequently, these correlations are unique to the SNL compressor. Furthermore, it is worth noting that the efficiency correlation was derived from total-to-static efficiency data (Wright et al., 2010). The correlations

are valid for modified flow coefficients ranging from 0.02 to 0.05, which Dyreby (2014) assumed to be the surge and choke points for the compressor, respectively. Furthermore, at the design point (at $N = N_{nom} = 75000$ rpm), the efficiency is 67.78% and the head coefficient is 0.4618 at a flow coefficient of 0.02971.

$$\eta^* = -0.7069 + 168.6\phi^* - 8089\phi^{*2} + 182725\phi^{*3} - 1.638e^6\phi^{*4} \quad (1)$$

$$\psi^* = 0.04049 + 54.7\phi^* - 2505\phi^{*2} + 53224\phi^{*3} - 498626\phi^{*4} \quad (2)$$

$$\phi^* = \phi\left(\frac{N}{N_{nom}}\right)^{0.2} = \frac{\dot{m}}{\rho_1 u_2 D_2^2}\left(\frac{N}{N_{nom}}\right)^{0.2} \quad (3)$$

$$\eta^* = \eta\left(\frac{N_{nom}}{N}\right)^{(20\phi^*)^5} \quad (4)$$

$$\psi^* = \psi\left(\frac{N_{nom}}{N}\right)^{(20\phi^*)^3} = \frac{w_{c.s}}{u_2^2}\left(\frac{N_{nom}}{N}\right)^{(20\phi^*)^3} \quad (5)$$

To facilitate the off-design analysis of a recompression cycle, Dyreby (2014) applied their correlations, but for an increased design efficiency and a different design speed, effectively scaling their performance curves geometrically to model a different compressor. Dyreby (2014) also assumed that the isentropic efficiency is equal to the total-to-static efficiency. In doing so, Dyreby (2014) assumed that the static and total fluid conditions are the same. From a cycle-level perspective, the velocities at the inlet and outlet of the components are relatively low, and it is generally acceptable to calculate fluid properties at the total conditions. However, within the turbomachines the fluid velocities increase significantly through the various flow channels, which may impact the fluid properties significantly, especially for sCO_2 compressors which operate near the critical point. Other literature employing Dyreby's correlations apply the same efficiency assumption, and include a study by Luu et al. (2017b), who analyzed a start-up strategy and loss of charge event for a hybrid solar and fossil fueled recompression cycle. To perform the work, Dyreby's correlations were used to configure the compressor component within the Dymola modelling and simulation software. Since Luu et al. (2017b) investigated fast transient cases, the moment of inertia for each compressor should have been taken into account. However, Luu et al. (2017b) do not provide any details. Thanganadar et al. (2020) also used Dyreby's correlations to compare the off-design and annual performance of a CSP plant incorporating TES and either a simply recuperated sCO_2 cycle, a recompression cycle, or a partial cooling cycle. Correa et al (2021) used Dyreby's correlations to study the off-design performance of a CSP plant incorporating the recompression cycle. More recently, Yang, Yang & Duan (2023) applied Dyreby's correlations to study the performance of a simple Brayton cycle under fluctuating

ambient temperatures and power demand scenarios.

1.3. Mean-line models

A common method for preliminary turbomachine design, before refinement using three-dimensional (3D) computational fluid dynamics (CFD) and testing, is to employ a mean-line analysis. In this analysis, the performance of the turbomachine is predicted by one-dimensional (1D) analysis of the mean fluid streamline using velocity triangles, the continuity equation, Euler turbomachine equation, and loss correlations. For additional information on the mean-line analysis method, the reader is referred to the literature in Japikse & Baines (1997) and Dixon & Hall (2014). For a review of loss correlations, the reader is referred to the work of Zhang et al. (2019), as well as the sources provided in Table 1 in Section 3.2.

Employing a mean line analysis, Lee (2016) developed the KAIST-TMD code for the design and performance prediction of radial sCO_2 compressors. KAIST-TMD is not publicly available, but Lee (2016) provide details of the methodology and loss correlations applied. The modelling methodology (excluding the solving algorithm) are similar to the methods applied in this work, with the main differences being the inclusion of inlet guide vanes in this work, and the model used for the vaneless space. Furthermore, Lee (2016) does not provide information about the vaned diffuser and volute model used, which could also be different to those used in this work. Finally, the impeller enthalpy loss set proposed by Oh et al. (1997) is employed in KAIST-TMD, which is different to the loss set used in this work.

Using KAIST-TMD, Lee (2016) designed a compressor for a recompression cycle coupled to a Sodium-cooled fast reactor, determining the required key geometry and resultant performance maps. Cho et al. (2019) used the KAIST-TMD to investigate the effect of backswept impellers on compressor performance. To evaluate similitude models for sCO_2 applications, Jeong et al. (2020) used KAIST-TMD to develop generic performance maps for sCO_2 compressors. None of the models tested were satisfactory (including the common ideal gas model), and they proposed that a modified version of the model proposed by Pham et al. (2016) be used. The model is not used in this work. Instead, this work adopts the use of isentropic head and efficiency vs. inlet volume flow rate curves, which remain (almost) the same for a given speed at different inlet conditions (Flownex SE, 2020).

AlFa CCD is another mean-line code for a radial compressor, developed by Ameli in 2017 (as cited by Ameli et al., 2018). AlFa CCD and the modelling methods applied to develop the code is not publicly available, but Ameli et al. (2018) mention that it employs the enthalpy loss correlation set proposed by Oh et al. (1997). Ameli et al. (2018) investigated the accuracy of the loss

correlations used in the code for sCO_2 applications by comparing total-to-total efficiency results with test data from the SNL compressor (it is unclear how total-to-total efficiency data were obtained since Wright et al. (2010) provide only total-to-static data). For a speed of 50 000 rpm, and if the skin friction correlation used to model losses is changed to one which takes surface roughness into account, Ameli et al. (2018) show that the results obtained fit the SNL experimental data well.

1.4. Other models

Other models found in literature include the performance maps for a radial compressor developed by Gong, et al. in 2016 (cited by Carstens, 2007), and for an axial compressor developed by Wang, et al in 2003 (cited by Dostal, Driscoll & Hejzlar, 2004). Carstens (2007) applied the radial compressor maps to investigate the transient response of a recompression cycle indirectly coupled to a nuclear reactor. Inertial effects were not modelled. Furthermore, an ideal gas-based similitude model was used to determine compressor performance at off-design conditions. Dostal et al. (2004) applied the axial compressor maps, developed using the AXIAL computer-aided engineering software from Concepts NREC, to study the off-design performance of a recompression cycle indirectly coupled to a nuclear reactor. It is unclear if a suitable similitude model was used to determine compressor performance at off-design conditions. Furthermore, to the best of the author's knowledge, this is the only work which considered axial compressors instead of radial compressors.

2. Scope of work

This current work presents the development of a verified mean-line code, and a method employing the code which may be used to size (obtain key geometry) and develop performance maps for radial sCO_2 compressors. The use of the code is then demonstrated by presenting the conceptual designs of two compressors for a proposed 50 MWe sCO_2-CSP plant in Southern Africa.

3. Model development

The models developed in this work were implemented in Engineering Equation Solver (EES) version 10.829 (Klein, 1993), which has built-in real fluid property data and uses the Newton-Raphson method to solve non-linear sets of equations, regardless of the order of input.

3.1. Governing equations

To understand the following text, it is necessary to introduce the system being modelled. Figure

1 provides a schematic of the compressors, showing the various elements and the mean streamline path, which is aligned with the shaft axis at the compressor inlet, and the radial direction at the impeller exit. To facilitate high efficiencies, each compressor features optional inlet guide vanes (IGVs) to introduce pre-whirl, backswept impellers, channel-type vaned diffusers (wedge shaped) and a volute. Figure 2 provides a Mollier diagram (enthalpy-entropy diagram) of the entire process. The diagram includes lines of constant total pressure for each node (or station), as well as a line of constant static pressure at the exit (station 5). Points are given for the actual fluid state at each station (red filled circles) as well as the ideal state if a process was isentropic (denoted by s). Additionally, points are given if the entire process was isentropic (denoted by ss) and if there were no external losses across the impeller (point $02.int$).

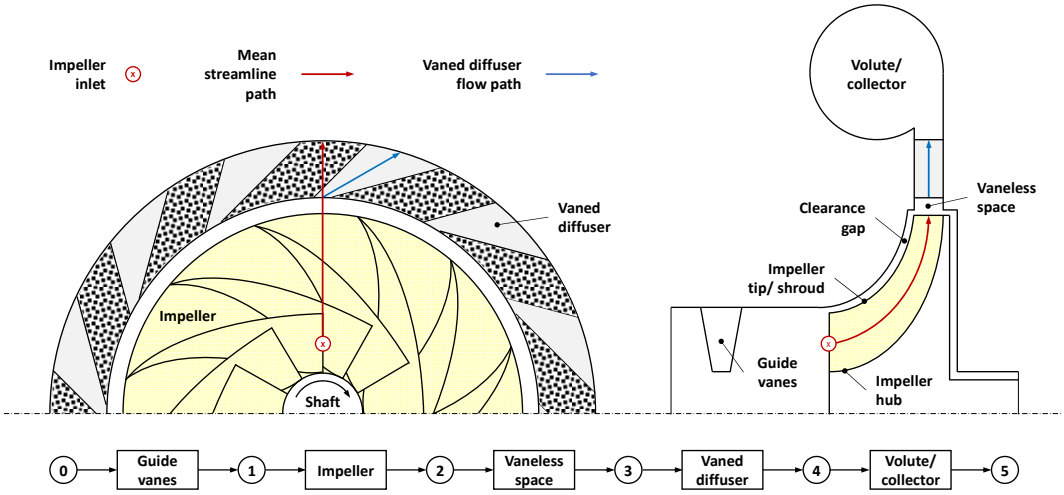

Figure 1: Schematic of compressor elements and mean streamline

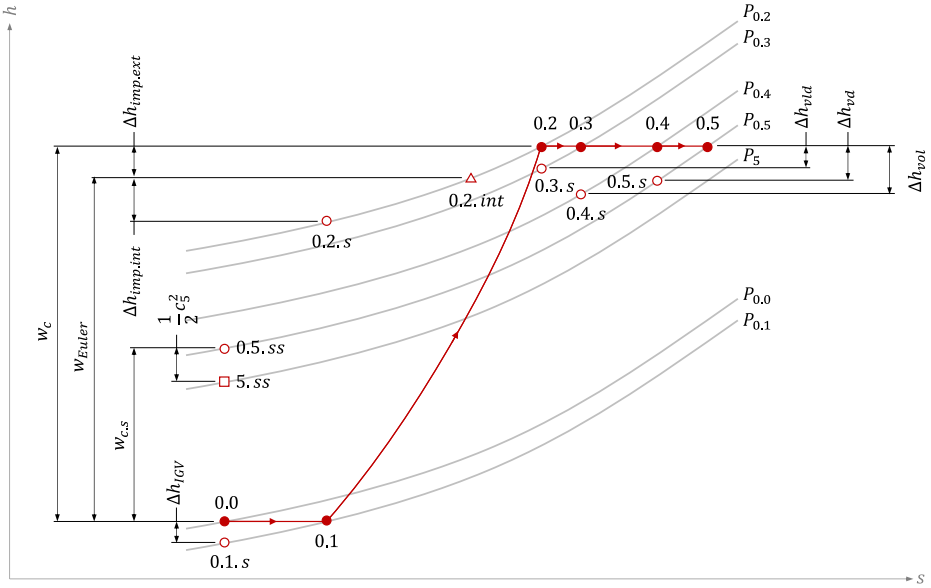

Figure 2: Mollier diagram of compressor

For all elements, the mass flow rate is given by:

$$\dot{m} = \rho A c \tag{6}$$

where A is the flow area normal to the absolute fluid velocity, either c or c_m. For a compression process, the impeller work (which will have a negative value) is equal to the rate of change of angular momentum multiplied by the angular velocity:

$$w_{Euler} = -\omega(r_2 c_{t.2} - r_1 c_{t.1}) \tag{7}$$

During this process, various losses occur which generates entropy. These include internal losses and external losses. Internal losses increase the required impeller work to obtain a required stagnation pressure rise when compared to an ideal process (compare the change in enthalpy from points 0.1 and $0.2.int$ with the change from points 0.1 to $0.2.s$). In contrast, external losses increase the required shaft work without affecting the impeller work. Enthalpy losses also occur through the other compressor elements, generating entropy and decreasing the overall efficiency of the compressor. The energy balance equations used in this work are given below. For the impeller:

$$h_{0.out.s} = h_{0.in} - w_{Euler} - \Delta h_{imp.int} \tag{8}$$

$$h_{0.out} = h_{0.in} - w_{Euler} + \Delta h_{imp.ext} \tag{9}$$

and for every other element:

$$h_{0.out.s} = h_{0.in} - \Delta h_{element} \tag{10}$$

$$h_{0.out} = h_{0.in} \tag{11}$$

where the enthalpy losses are calculated using correlations. For all elements, using real gas fluid property relationships and noting that entropy may be determined at either static or total conditions, the outlet stagnation conditions are determined given the inlet static conditions:

$$s_{in} = f(P_{in}, T_{in}) \tag{12}$$

$$s_{out.s} = s_{in} \tag{13}$$

$$P_{0.out} = f(h_{0.out.s}, s_{out.s}) \tag{14}$$

$$T_{0.out} = f(h_{0.out}, P_{0.out}) \tag{15}$$

At each node, the relationship between total and static enthalpy, and fluid properties are determined using real gas fluid property relationships:

$$h_0 = h + \frac{1}{2}c^2 \tag{16}$$

$$h, \rho, v, ss = f(P, T) \tag{17}$$

Finally, the compressor isentropic and real specific work, and efficiencies are given by:

$$w_{c.s} = h_{0.0} - h_{0.5.ss} \tag{18}$$

$$w_c = h_{0.0} - h_{0.5} \tag{19}$$

$$\eta_{TS} = \frac{h_{0.0} - h_{5.ss}}{w_c} \tag{20}$$

$$\eta_{TT} = \frac{w_{c.s}}{w_c} \tag{21}$$

3.2. Correlations

The correlations and models applied in this work include: (i) enthalpy loss correlations, used to model the inlet guide vanes, the impeller, the vaneless space and the vaned diffuser; (ii) a static pressure recovery model, used to model the volute; and (iii) a slip factor model, used to model slip at the impeller exit. Since the constraints of this paper prevent a detailed presentation of the correlations applied in this work, Table 1 provides a summary with references to the source material. For (ii), the enthalpy loss across the element in Equation (10) are solved to obtain the required static pressure recovery.

Table 1: Summary of correlations and models applied in this work

	Loss/ Model	**Source**
	Inlet guide vanes	(Galvas, 1973)
Internal losses	Skin friction	Jansen (as cited by Ameli et al., 2018; Harrison, 2020)
	Impeller blade loading	(Aungier, 1995)
	Hub to shroud (for shrouded impellers)	(Aungier, 1995)
	Mixing	(Aungier, 1995)
	Clearance (for unshrouded impellers)	Jansen (as cited by Zhang et al., 2019)
	Incidence	(Aungier, 2000)
	Entrance diffusion	(Aungier, 1995)
	Choke	(Aungier, 1995)
	Shock	(Aungier, 1995)
External losses	Disk friction	Daily & Nece (as cited by Zhang et al., 2019)
	Recirculation	Coppage & Dallenbach (as cited by Zhang et al., 2019)
	Leakage (for unshrouded impellers)	(Aungier, 1995)
	Vaneless space (friction)	Based on Jansen (as cited by Ameli et al., 2018)
	Vaned diffuser (incidence)	Aungier (as cited by Zhang et al., 2019)
	Vaned diffuser (friction)	Based on Jansen (as cited by Ameli et al., 2018)
	Volute pressure recovery	Japikse & Baines (1997)
	Slip factor	Wiesner (1967)

4. Model verification

Using the inputs provided in Table 2, Figure 3 compares the results obtained using the mean-line model developed in this work with SNL test data from Wright et al. (2010). Additionally, using the same code, the current method is compared to Dyreby's method by replacing the enthalpy loss correlations with Dyreby's correlations. This approach forces the performance curves to match Dyreby's correlations, but provides more information about the various fluid properties, velocities and losses throughout the compressor. The current method agrees well with the isentropic head ($\Delta h_{0.s} = -w_{c.s}$) test data. At low mass flow rates, the model is slightly optimistic. At both low speeds and high mass flow rates, the model is slightly conservative. Dyreby's method, in comparison, is conservative across all speeds and mass flow rates. When comparing total-to-static efficiencies, the peak efficiencies obtained with the current method agree well with the test data. However, the efficiencies are optimistic for decreasing mass flow rates, and conservative for increasing mass flow rates. This result is welcomed, given that the model developed in this work includes a volute, whereas the SNL main compressor does not have volute, only a collection chamber (this collection chamber is modelled like a volute due to a lack of detailed information). It is therefore expected that there will be greater static pressure recovery at lower flow rates, and greater losses at higher flow rates. Dyreby's method, in comparison, is conservative but the trends agree well with the test data. Although not presented here, when using Dyreby's correlations, $\Delta h_{imp.ext}$ is observed to be negative for some cases at higher flow rates. At these higher flow rates, this may contribute towards the observed efficiencies being higher than those obtained using the current method. However, it is not physically possible for $\Delta h_{imp.ext}$ to be negative. This observation highlights one of the shortcomings of applying Dyreby's correlations.

Table 2: Inputs for model verification study

Specification	Units	Value
Known, from Wright et al. (2010)		
Number of full blades	-	6
Number of splitter blades	-	6
Number of vaned diffuser channels	-	17
Blade angle at impeller inlet	°	50.0
Blade angle at impeller exit (backswept)	°	50.0
Vaned diffuser angle at diffuser inlet	°	71.5
Hub radius	mm	2.54
Shroud radius	mm	9.37
Impeller exit radius	mm	18.68
Tip clearance	mm	0.254

Specification	Units	Value
Blade thickness	mm	0.76
Blade height at exit	mm	1.71
Nominal mass flow rate	kg/s	3.53
Total pressure at inlet	kPa	7687
Total temperature at inlet	°C	32.15
Assumed		
Ratio of splitter blade to full blade meridional length	-	0.5
Blade angle at impeller inlet (at hub, mean position and shroud)	°	50.0
Vaned diffuser inlet diameter	mm	40
Vaned diffuser exit diameter	mm	75
Vaned diffuser height	mm	1.71
Collector exit diameter	mm	29.89

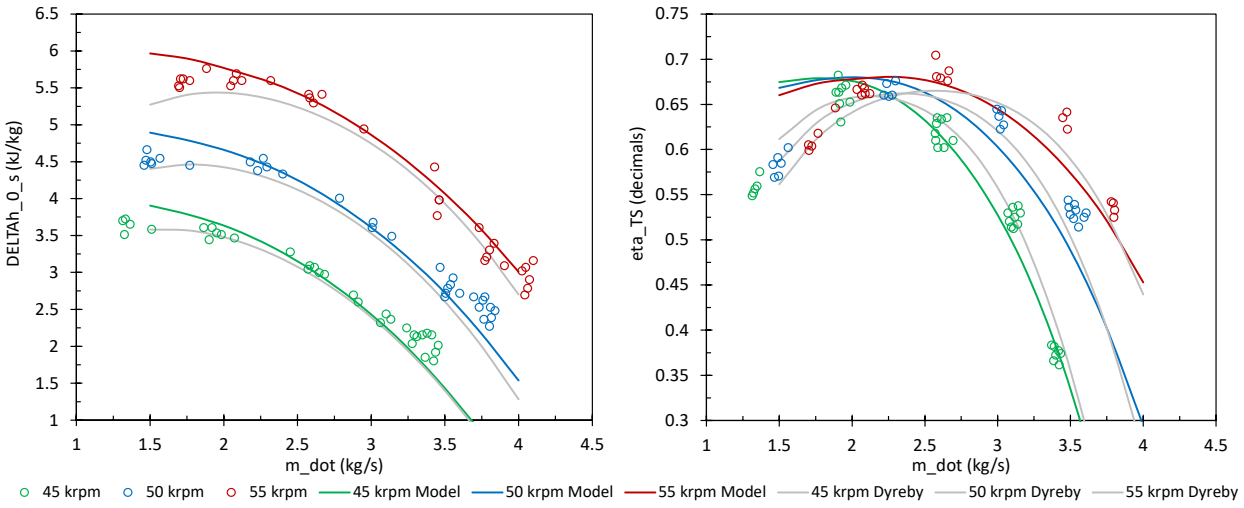

Figure 3: Comparison of current method to Dyreby method and SNL test data from Wright et al. (2010)

5. Design method

Conceptual compressor designs were developed to serve as the low pressure compressor (LPC), high pressure compressor (HPC) and recompression compressor (RCC) for a recompression cycle with intercooling and reheating, which forms part of a proposed 50 MWe sCO_2-CSP plant in Southern Africa. The boundary conditions for the compressors were determined in a recent study by the authors (du Sart, Rousseau & Laubscher, 2024). The design criteria are provided in Table 3 in Section 6 for the LPC and HPC (the design criteria and final results for the RCC are excluded due to the constraints of this paper).

Initially, careful consideration should go into choosing a shaft layout for the power cycle and determining appropriate operating speeds. For this work, the specific speed-diameter diagram

from Balje (1981) was used to determine suggested operating speeds for each compressor which could lead to efficient designs. A marked-up diagram is provided in Figure 4 in Section 6, and the definitions for specific speed and specific diameter are given below:

$$n_s = \frac{\omega \left(\frac{\dot{m}}{\rho_0}\right)^{\frac{1}{2}}}{(h_{5.ss} - h_{0.0})^{\frac{3}{4}}} \tag{22}$$

$$d_s = \frac{D_1 (h_{5.ss} - h_{0.0})^{\frac{1}{4}}}{\left(\frac{\dot{m}}{\rho_0}\right)^{\frac{1}{2}}} \tag{23}$$

Given the required boundary conditions and suggested operating speeds, the mean-line code developed in this work was then used to determine the geometry of each compressor. To do so, the mass flow rate, inlet temperature and pressure, and pressure ratio were set, and the DIRECT multiparameter optimization algorithm (Jones, Perttunen & Stuckman, 1993) within EES was applied to minimize the following objective function:

$$OBJECTIVE = X_1 \left(\left| \frac{\eta_{TT} - \eta_{TT.target}}{\eta_{TT.target}} \right| \right) + X_2 \left(\left| \frac{\eta_{TS} - \eta_{TT.target}}{\eta_{TT.target}} \right| \right) \tag{24}$$

where the weights X_1 and X_2 were set to 0.9 and 0.1, respectively. By applying this objective function, a global solution is obtained where the target total-to-total efficiency is realized, and the total-to-static efficiency is maximized. Note that if the total-to-total efficiency was set instead, there would be many local solutions. From observations made during this work, many of these local solutions result in a compressor which has undesirable off-design performance characteristics. The optimised variables are listed in Table 3 in Section 6 with allowable ranges. According to various literature, the ranges considered are typical for well-designed compressors. Two fixed variables, namely the number of blades and vaned diffuser channels were chosen to reduce computational expense and the risk of numerical errors occurring during the calculation. However, these variables could be included in the optimisation. In selecting the number of blades, from the geometry of the SNL main compressor and recompression compressor, it was observed that a linear plot of the ratio of compressor blades to impeller diameter vs. impeller diameter has a gradient of 0.05. The selected number of blades provides a similar result. The selected number of vaned diffuser channels are roughly 50% more than the number of blades, similar to the main compressor at SNL.

Once the geometries were determined, isentropic head and efficiency curves were generated using the mean-line code. These curves were generated at the nominal design speed only for a volume flow rate ranging from 40% to 150% of the design volume flow rate. The results were then

scrutinized to determine representative flow coefficient $\left(\phi = \frac{\dot{m}}{\rho_1 u_2 D_2^2}\right)$ ranges for each compressor which prevents surge and choke. Additional performance curves were then generated at different speeds using the determined flow coefficient ranges.

Finally, representative CAD models of the impellers were generated to obtain inertia estimates. A mean blade thickness of $0.01D_2$ was assumed and Aluminum 6061 was used for impeller material, based off the SNL compressors.

In closing, note that the design process could be iterative for three reasons: (i) If the obtained total-to-total efficiency is not acceptable, the fixed variables may need to be changed, or included in the optimisation process; (ii) If the resultant head curve is too flat or steep, some of the optimized variables may need to be fixed instead e.g. adjusting the blade angle at the impeller exit to obtain a more flat or steep curve (iii) When using the performance curves as part of a cycle analysis, the analysis may call for compressor curves which are different in shape or have a wider operating envelope. Again, strategically fixing some of the optimized variables may solve the problem. However, if the compressor performance or cycle analysis is still unsatisfactory, two compressors in series, or alternative shaft layouts and speeds may need to be considered.

6. Results

Figure 4 shows the preliminary sizing analysis performed to obtain estimates for the impeller diameters, operating speeds, and shaft layout. The preliminary markers were plotted for an operating speed of 9000 rpm. To plot these markers, the density was calculated at total temperature and pressure conditions, and the term $(h_{5.ss} - h_{0.0})$ in Equations (22) and (23) was approximated using the isentropic head from the cycle analysis $(\Delta h_{0.s} = h_{0.5.ss} - h_{0.0})$. All the markers fall within the recommended range for radial or mixed flow machines, consequently a single shaft layout operating at 9000 rpm was selected, which requires a 3:1 speed increasing gearbox given a synchronous frequency of 50 Hz i.e. 3000 rpm in Southern Africa. The clear filled markers were plotted after the design process. Compared to the preliminary markers for the LPC and HPC, they are shifted slightly down and towards the right. This is expected to some extent since $h_{0.s} \geq (h_{5.ss} - h_{0.0})$, and the markers shift down and towards the right with decreasing values of $(h_{5.ss} - h_{0.0})$. A clear marker for the RCC is not provided because a suitable design was not obtained at 9000 rpm (a suitable design was obtained at 24 000 rpm and for two compressors operating in series at 9000 rpm). The result is not surprising, since the preliminary marker for the RCC lies close to the outskirts of the recommended range, near lower efficiency contours. Despite being developed using ideal gas based data and approximations, these results show that the specific speed-diameter diagram from Balje (1981) may be used in the preliminary design phase.

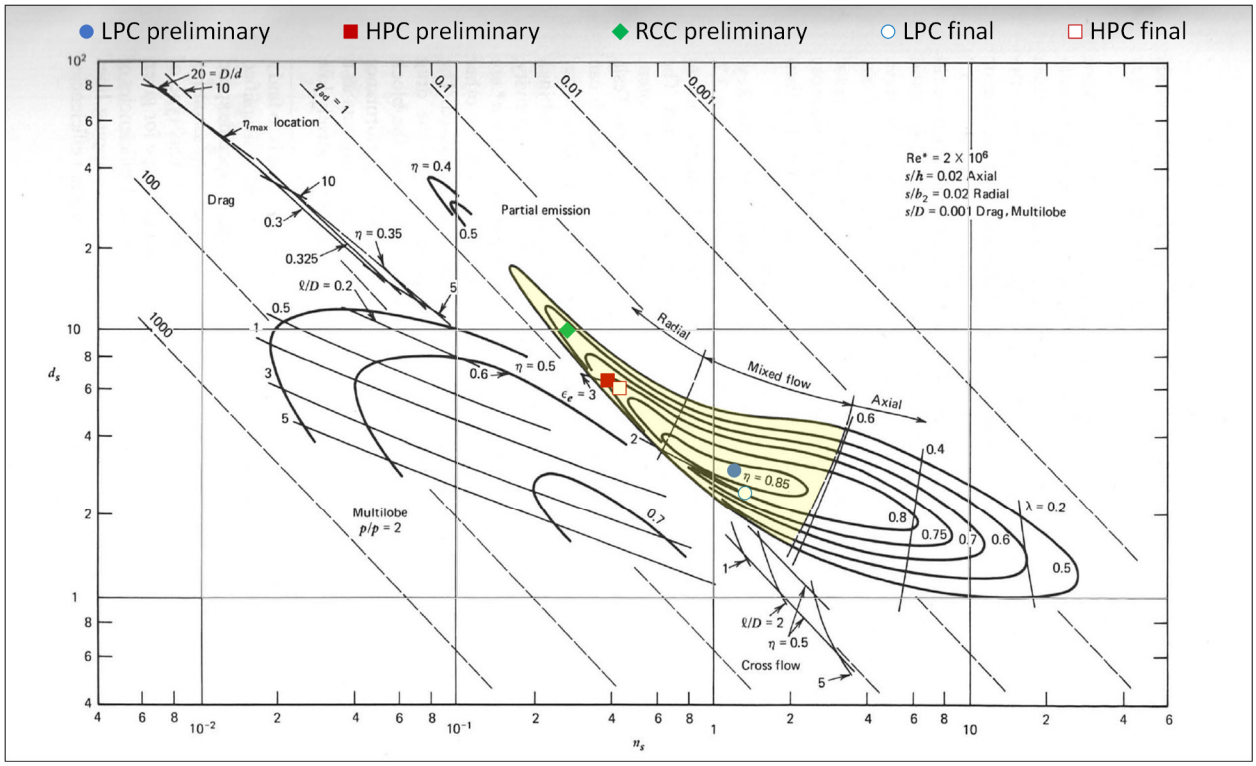

Figure 4: Marked-up specific speed-diameter diagram, from Balje (1981)

Table 3 provides the calculated geometry and performance for the LPC and HPC, Figure 5 provides the performance maps, and Figure 6 provides images of representative CAD models which were constructed to obtain inertias. The images are shown without shrouds to provide an unobstructed view of the blades. However, the actual compressors feature shrouds to mitigate clearance and leakage losses.

Principally, the results show that the design method followed produces realistic geometry and performance curves. Furthermore, the compressors can operate over a wide range of speeds and flow conditions, and the curves provide clear choke and surge lines. Secondly, the results confirm that a commonly assumed isentropic efficiency of 89% is achievable for sCO_2 radial compressors, provided inlet swirl is included in the design process. Thirdly, the results show that the three compressors vary significantly in geometry and performance, further suggesting that it would be un-wise to use Dyreby's correlations to model various compressors, all with different design criteria. Finally, by performing a mean-line analysis, there is additional data which can be analyzed to scrutinize the validity of the compressor model used. For example, Figure 7 shows a plot of all the minimum static temperatures within the compressors. For the HPC, when operating at the highest speed and flow rate, the model predicts that a two-phase flow state may be encountered which is of course not desirable.

Table 3: Summary of conceptual compressor designs

Specification	Units	LPC	HPC
Design criteria			
Mass flow rate	kg/s	397	397
Total pressure at inlet	kPa	7353	9768
Total temperature at inlet	°C	45	45
Total pressure ratio	-	1.356	2.560
Total-to-total efficiency (target)	%	89	89
Fixed variables			
Number of full blades	-	19	19
Number of vaned diffuser channels	-	28	28
Nominal design speed	rpm	9000	9000
Optimised variables			
Hub to shroud radius ratio	-	[0.3, 0.6]	
Shroud to tip radius ratio	-	[0.35, 0.65]	
Vaned diffuser inlet to impeller exit radius ratio	-	[1.025, 1.075]	
Vaned diffuser exit to inlet radius ratio	-	[1.25, 1.75]	
Inlet swirl angle	°	[0, 35]	
Blade angle at impeller inlet (mean position)	°	[25, 50]	
Blade angle at impeller exit (backswept)	°	[25, 50]	
Calculated geometry			
Inlet swirl angle	°	35	17.5
Blade angle at impeller inlet (at hub, mean position and shroud)	°	25.5	37.5
Blade angle at impeller exit (backswept)	°	49.5	37.5
Vaned diffuser mean flow path angle	°	60.5	68.5
Blade height at exit; vaned diffuser height	mm	29.280	8.334
Inlet guide vane upstream diameter	mm	200.7	137.0
Hub diameter	mm	70.0	70.5
Shroud diameter	mm	232.6	157.6
Impeller exit diameter	mm	358.0	450.2
Vaned diffuser inlet diameter	mm	384.9	483.9
Vaned diffuser exit diameter	mm	672.6	846.8
Volute exit diameter	mm	211.3	105.5
Axial length	mm	115.80	91.33
Inertia	kg-mm^2	78 968	181 881
Performance at design point			
Minimum flow coefficient	-	0.0382	0.0084
Maximum flow coefficient	-	0.1339	0.0314
Volume flow rate at inlet	m^3/s	2.062	0.8986
Isentropic head	kJ/kg	11.61	27.30
Total-to-total efficiency (actual)	%	88.79	89.07
Total-to-static efficiency	%	80.59	80.19
Compressor power	MW	-5.193	-12.166

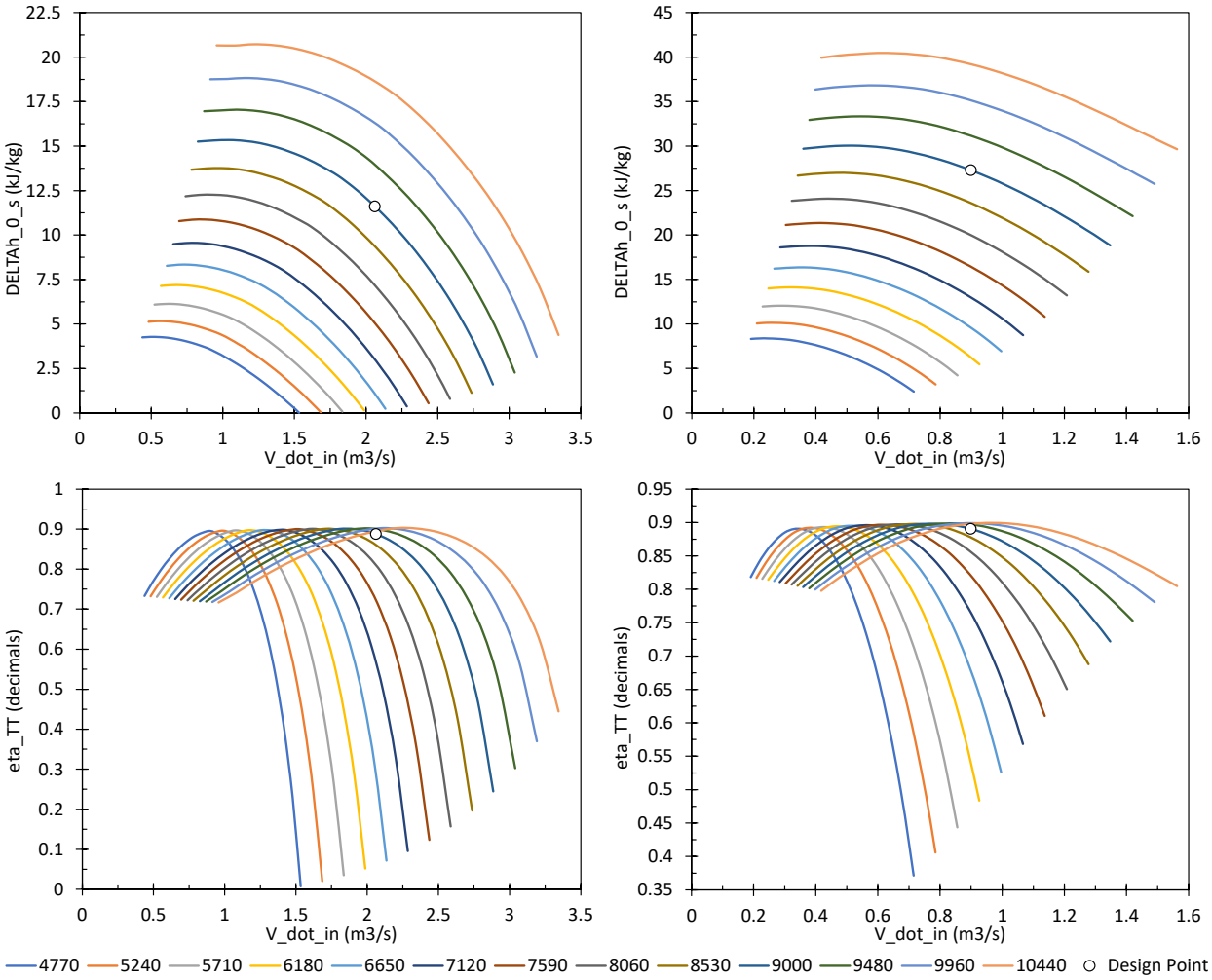

Figure 5: Performance maps of LPC (left) and HPC (right)

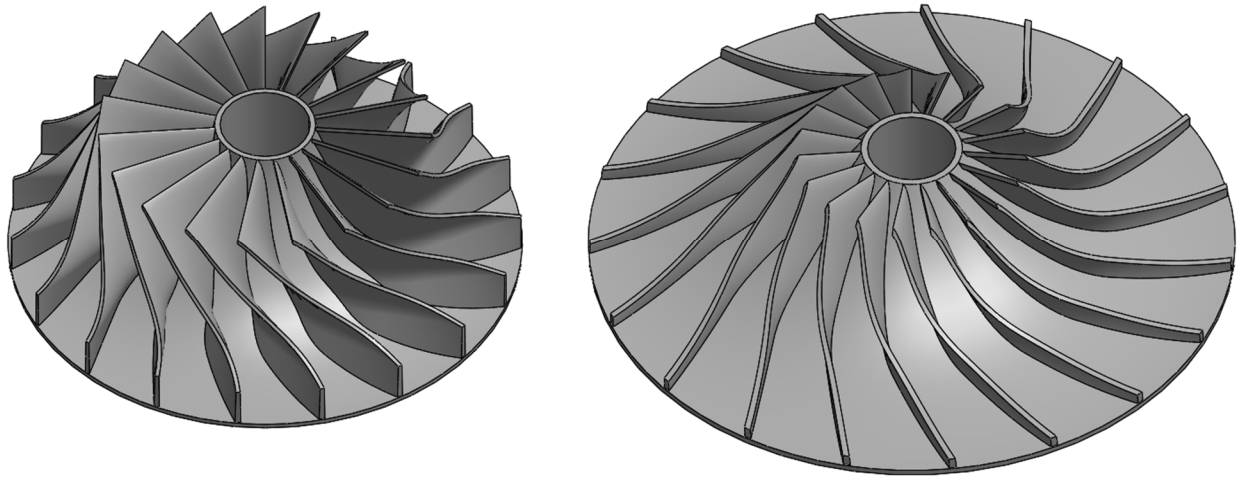

Figure 6: CAD models of LPC (left) and HPC (right) with shrouds removed

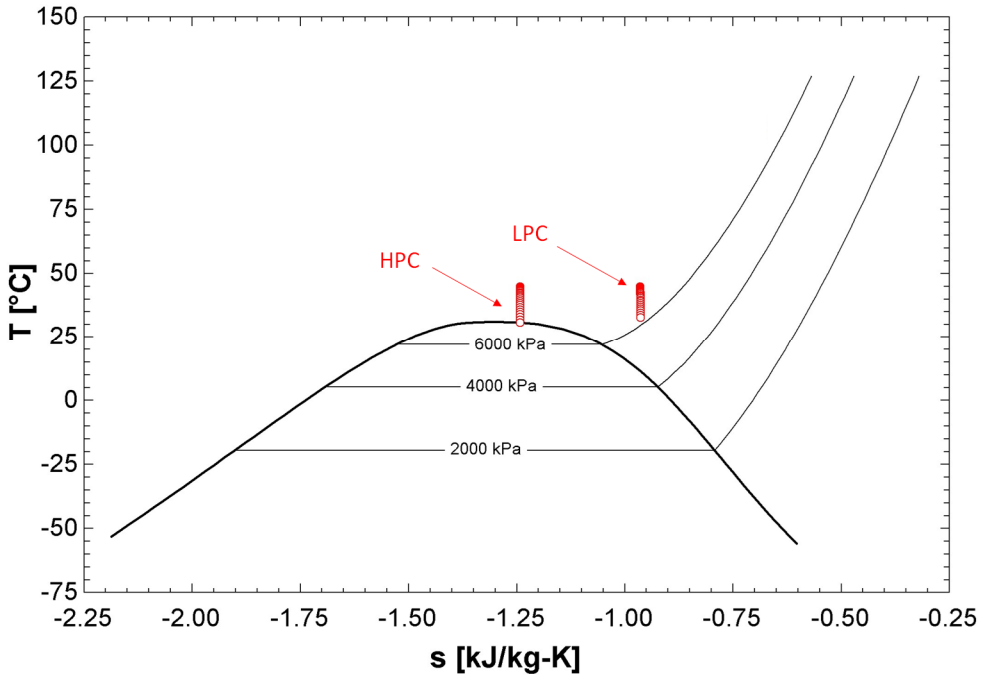

Figure 7: T-s diagram showing minimum static temperatures within LPC and HPC

7. Summary and conclusions

This work discussed the various steady state and dynamic models found in literature for sCO_2 radial compressors. With the exception of KAIST-TMD, which is not available in the public domain or fully documented, there are no suitable dynamic models, and most researchers apply Dyreby's correlations to model sCO_2 compressors. However, this work has shown that although useful, there are shortcomings to using Dyreby's correlations. Given this, a mean-line code was developed, verified and used to size (obtain key geometry) and develop performance maps for radial sCO_2 compressors which include inlet guide vanes, a vaned diffuser and a volute. The fundamental balance equations and the correlations used in the development of the mean-line code was presented, and case studies were presented to demonstrate how the code can be used to develop conceptual compressor designs. In comparison to other methods used to model sCO_2 compressors in literature, the presented method is suitable for dynamic studies since it considers real gas fluid properties in the performance characterization of the compressor for on and off-design cases, and an estimate for the compressor inertia is determined. The method employed in this work may be used in future studies where compressor curves are required, particularly for studies investigating fast transient cases. Future work will include using the compressor maps presented here as part of an ongoing study to develop a fully dynamic model of a proposed 50 MWe sCO_2-CSP tower plant in Southern Africa.

Acknowledgements

The authors would like to thank the Department of Higher Education and Training of South Africa for funding this research through the New Generation of Academics Programme (nGAP). The authors would also like to acknowledge the Applied Thermal Process Modelling (ATProM) Research Unit at the University of Cape Town, of whom the authors are members, for providing the environment in which to complete this research.

References

Ameli, A., Turunen-saaresti, T., Grönman, A. & Backman, J. 2018. Compressor design method in the supercritical CO2 applications. *The 6th International Symposium - Supercritical CO2 Power Cycles*.

Aungier, R.H. 1995. Mean streamline aerodynamic performance analysis of centrifugal compressors. *Journal of Turbomachinery*. 117(3):360–366. DOI: 10.1115/1.2835669.

Aungier, R.H. 2000. *Centrifugal Compressors: A Strategy for Aerodynamic Design and Analysis*. New York: ASME Press. DOI: 10.1115/1.800938.

Balje, O.E. 1981. *Turbomachines: A Guide to Design, Selection, and Theory*. New York: John Wiley & Sons.

Binotti, M., Astolfi, M., Campanari, S., Manzolini, G. & Silva, P. 2017. Preliminary assessment of sCO2 cycles for power generation in CSP solar tower plants. *Applied Energy*. 204:1007–1017. DOI: 10.1016/j.apenergy.2017.05.121.

Brun, K., Friedman, P. & Dennis, R. 2017. *Fundamentals and Applications of Supercritical Carbon Dioxide (SCO2) Based Power Cycles*.

Carstens, N. 2007. Control strategies for supercritical carbon dioxide power conversion systems. Massachusetts Institute of Technology.

Cho, S.K., Bae, S.J., Jeong, Y., Lee, J. & Lee, J.I. 2019. Direction for high-performance supercritical CO2 centrifugal compressor design for dry cooled supercritical CO2 Brayton cycle. *Applied Sciences (Switzerland)*. 9(19). DOI: 10.3390/app9194057.

Correa, F., Barraza, R., Soo Too, Y.C., Vasquez Padilla, R. & Cardemil, J.M. 2021. Optimized operation of recompression sCO2 Brayton cycle based on adjustable recompression fraction under variable conditions. *Energy*. 227. DOI: 10.1016/j.energy.2021.120334.

Dixon, S.L. & Hall, C.A. 2014. *Fluid Mechanics and Thermodynamics of Turbomachinery Seventh Edition Fluid Mechanics and Thermodynamics of Turbomachinery Seventh Edition*. 7th ed. Oxford: Elsevier Inc.

Dostal, V., Driscoll, M.J. & Hejzlar, P. 2004. A Supercritical Carbon Dioxide Cycle for Next Generation Nuclear Reactors. Massachusetts Institute of Technology.

Dyreby, J.J. 2014. Modeling the Supercritical Carbon Dioxide Brayton Cycle with Recompression. WISCONSIN-MADISON.

Flownex SE. 2020. *Flownex Library Manual*.

Galvas, M. 1973. *Fortran program for predicting off-design performance of centrifugal compressors*. Washington DC.

Harrison, H.M. 2020. Development and Validation of a New Method To Model Slip and Work Input for Centrifugal Compressors. Purdue University.

Japikse, D. & Baines, N.C. 1997. *Introduction to Turbomachinery*. Concepts ETI Inc. and Oxford University Press.

Jeong, Y., Son, S., Cho, S.K., Baik, S. & Lee, J.I. 2020. Evaluation of supercritical CO2 compressor off-design performance prediction methods. *Energy*. 213:119071. DOI: 10.1016/j.energy.2020.119071.

Jones, D.R., Perttunen, C.D. & Stuckman, B.E. 1993. Lipschitzian Optimization Without the Lipschitz Constant. *Journal of optimization theory and application*. 79(1):157–181. DOI: https://doi.org/10.1007/BF00941892.

Klein, S.A. 1993. Development and integration of an equation-solving program for engineering thermodynamics courses. *Computer Applications in Engineering Education*. 1(3):265–275. DOI: 10.1002/cae.6180010310.

Kulhanek, M. & Dostal, V. 2011. Thermodynamic Analysis and Comparison of Supercritical Carbon Dioxide Cycles. In *Supercritical CO2 Power Cycle Symposium*. Boulder.

Lee, J. 2016. Study of improved design methodology of S-CO2 power cycle compressor for the next generation nuclear system application. Korea Advanced Institute of Science and Technology. Available: https://kdrm.kaist.ac.kr/ezpdfwebviewer/ezpdf/customLayout.jsp?encdata=67D4CD8135C7372A42DB0940C33C3EA11F56B0C612D0A8D3799BF481C377949DE464993BE0419278598BD59B7D4A0373654623C1456D6BC18194BAD1257817965B00F5FD41B0997C&lang=ko#.

Luu, M.T., Milani, D., McNaughton, R. & Abbas, A. 2017a. Analysis for flexible operation of supercritical CO2 Brayton cycle integrated with solar thermal systems. *Energy*. 124:752–771. DOI: 10.1016/j.energy.2017.02.040.

Luu, M.T., Milani, D., McNaughton, R. & Abbas, A. 2017b. Dynamic modelling and start-up operation of a solar-assisted recompression supercritical CO2 Brayton power cycle. *Applied Energy*. 199:247–263. DOI: 10.1016/j.apenergy.2017.04.073.

Neises, T. & Turchi, C.S. 2014. A comparison of supercritical carbon dioxide power cycle configurations with an emphasis on CSP applications. *Energy Procedia*. 49:1187–1196. DOI: 10.1016/j.egypro.2014.03.128.

Neises, T. & Turchi, C.S. 2019. Supercritical carbon dioxide power cycle design and configuration optimization to minimize levelized cost of energy of molten salt power towers operating at 650 °C. *Solar Energy*. 181(November 2018):27–36. DOI: 10.1016/j.solener.2019.01.078.

Oh, H.W., Yoon, E.S. & Chung, M.K. 1997. An optimum set of loss models for performance prediction of centrifugal compressors. *Proceedings of the Institution of Mechanical Engineers, Part A: Journal of Power and Energy*. 211:331–338. DOI: 10.1243/0957650971537231.

Osorio, J.D., Hovsapian, R. & Ordonez, J.C. 2016. Dynamic analysis of concentrated solar supercritical CO2-based power generation closed-loop cycle. *Applied Thermal Engineering*. 93:920–934. DOI: 10.1016/j.applthermaleng.2015.10.039.

Padilla, R.V., Benito, R.G. & Stein, W. 2015. An Exergy Analysis of Recompression Supercritical CO2 Cycles with and without Reheating. *Energy Procedia*. 69:1181–1191. DOI: 10.1016/j.egypro.2015.03.201.

Pham, H.S., Alpy, N., Ferrasse, J.H., Boutin, O., Tothill, M., Quenaut, J., Gastaldi, O., Cadiou, T., et al. 2016. An approach for establishing the performance maps of the sc-CO2 compressor: Development and qualification by means of CFD simulations. *International Journal of Heat and Fluid Flow*. 61:379–394. DOI: 10.1016/j.ijheatfluidflow.2016.05.017.

du Sart, C.F., Rousseau, P. & Laubscher, R. 2024. Comparing the partial cooling and recompression cycles for a 50 MWe sCO2 CSP plant using detailed recuperator models. *Renewable Energy*. DOI: 10.1016/j.renene.2024.119980.

Seidel, W. 2010. Model developmenet and annual simulation of the supercritical carbon dioxide Brayton cycle for concentrating solar power applications. University of Wisonsin - Madison.

Thanganadar, D., Fornarelli, F., Camporeale, S., Asfand, F. & Patchigolla, K. 2020. Analysis of design, off-design and annual performance of supercritical CO2 cycles for csp applications. *Proceedings of the ASME Turbo Expo*. 11:1–9. DOI: 10.1115/GT2020-14790.

Turchi, C.S., Ma, Z., Neises, T.W. & Wagner, M.J. 2013. Thermodynamic study of advanced supercritical carbon dioxide power cycles for concentrating solar power systems. *Journal of Solar Energy Engineering, Transactions of the ASME*. 135(4):1–7. DOI: 10.1115/1.4024030.

Wiesner, F.J. 1967. A review of slip factors for centrifugal impellers. *Journal of Engineering for Gas Turbines and Power*. 89(4):558–566. DOI: 10.1115/1.3616734.

Wright, S.A., Radel, R.F., Vernon, M.E., Rochau, G.E. & Pickard, P.S. 2010. *Operation and Analysis of a Supercritical CO2 Brayton Cycle*. Albuquerque. DOI: https://doi.org/10.2172/984129.

Yang, J., Yang, Z. & Duan, Y. 2023. Design Optimization and Operating Performance of S-CO2 Brayton Cycle under Fluctuating Ambient Temperature and Diverse Power Demand Scenarios. *Journal of Thermal Science*. 32. DOI: 10.1007/s11630-023-1839-2.

Zhang, C., Dong, X., Liu, X., Sun, Z., Wu, S., Gao, Q. & Tan, C. 2019. A method to select loss correlations for centrifugal compressor performance prediction. *Aerospace Science and Technology*. 93:105335. DOI: 10.1016/j.ast.2019.105335.